Hindawi
Shock and Vibration
Volume 2021, Article ID 6670276, 13 pages
https://doi.org/10.1155/2021/6670276

Research Article

Optimization and Application of Spacing Parameter for Loosening Blasting with 24-m-High Bench in Barun Open-Pit Mine

Zuoming Yin [1], Desheng Wang [1], Xuguang Wang [2], Zhiheng Dang [1] and Wantao Li [3]

[1] *Shool of Civil & Resource Engineering, University of Science and Technology Beijing, Beijing 100083, China*
[2] *Beijing General Research Institute of Mining & Metallurgy, Beijing 100070, China*
[3] *Hebei Iron and Steel Group Mining Company Sijiaying North Branch, Tangshan, Hebei 063000, China*

Correspondence should be addressed to Desheng Wang; wds812123@163.com

Received 12 December 2020; Revised 18 January 2021; Accepted 1 February 2021; Published 13 February 2021

Academic Editor: Junfei Zhang

In view of the near slope blasting in Barun open-pit mine, which has merged sublevel mining, the operation safety conditions of middle-sized and large equipment in the second phase expansion are poor and need urgent improvement. To increase the efficiency of expansion and reduce costs, a 24-m-high bench and large spacing parameter for loosening blasting are proposed. The analysis of the physical mechanism of the stress wave attenuation in the rock indicates that the cylindrical charge is equivalent to several spherical charges. Considering the pressure attenuation, reflection, transmission, and superposition of the spherical charge after the equivalence, a double exponential function correction equation of the stress wave attenuation is obtained based on the Mises strength criterion. The stress of any point in the rock medium with various spacing parameter is obtained by calculation. ANSYS/LS-DYNA was used to simulate and study the stress distribution of a 24-m-high bench with various spacing parameter. Meanwhile, the accuracy of the correction equation was verified. The parameters of the high-bench blasting with good effect and low cost were determined to be 15 m × 5.5 m, and field tests were carried out. Results show that the large spacing parameter for 24-m-high bench loosening blasting in Barun open-pit mine is efficient and economical in medium-hard rock blasting. This study provides a reference for the practical exploration of the expansion of high benches in open-pit mines in China. The calculation error of the corrected double exponential function is near the numerical simulation result. It is suitable for all kinds of professional designers.

1. Introduction

Most metal mines in China use 10 m to 12 m bench heights. With the advancement of open-pit mining technology, complete sets of large-scale equipment have improved the equipment level of mines [1–4] and the basic conditions to increase the bench height. At present, the upper bench of Barun open-pit mine is temporarily supported. The conventional bench-by-bench method of leaning on near slope blasting faces problems, such as steep slopes, narrow expansion sites, and difficulty in ensuring the safety of large equipment operations. Therefore, a technical solution that uses large spacing parameter for loosening blasting with a 24-m-high bench to expand the siding is proposed, and the need for high efficiency and low cost must be urgently addressed.

According to Livingston's blasting funnel theory, loosening blasting is a kind of blasting technology that breaks the medium without throwing [5]. By adjusting the spacing parameter, the blasting effect can be improved and the unit consumption of explosives can be reduced. Scholars have used numerical calculation methods to find that the spatial stress distribution is uniform when spacing parameters are between 1.7 and 3.7, which are conducive to rock fragmentation. The analysis of the changes in blasting conditions and the rock breaking mechanism caused by the change of spacing parameter indicates that it can be as high as 3 to 8. The reasonable spacing parameter for loosening blasting is from 1.5 to 2.0 [6–9]. Li et al. used a cement mortar model to study the influence of spacing parameter on the crack penetration time between bench blasting holes and concluded that a large spacing parameter delays the crack penetration time and improves the energy utilization rate of the explosive and the blasting effect [10]. Research on loosening blasting under homogeneous rock mass conditions with large spacing parameter and the influence of joints and fissures on blasting has produced many results [11–14]. However, the study of large spacing parameters for loosening blasting is limited in the case of steps and large resistance lines. The increase in the resistance line of the bench may produce large blocks, which subsequently affect the shovel loading. The increase in the charge of combined blasting will increase the mining cost and cause other unfavorable factors, such as the impact of blasting vibration, the increase of the large blocks rate, and the increase of the distance of flying stones. Therefore, the loosening blasting of a high bench with large spacing parameter must analyze the action mechanism of cylindrical charge and the dynamic response of rocks. The stress state of the rock medium at different resistance lines can reasonably control the size of blasting vibration and the rate of large blocks to achieve refined blasting. Raina et al. defined and determined the impulse pressure and time to make the application of fly-rock prediction equations highly scientific [15]. Singh et al. evaluated and analyzed the blasting delay time, the borehole depth, the charging structure, and other influencing factors through digital image analysis to reduce the bulk rate and improve the blasting effect [16]. Zhong et al. obtained a precise time delay by using a digital electronic detonator based on energy distribution theory of explosive charge in the rock mass and calculated the reasonable delay time interval between blasting holes; the effectiveness of the approach was proven by production practice [17]. Iwano et al. reproduced the vibration waveforms in delay blasting from a seed waveform recorded in single-shot blasting. The optimum delay interval determined accurately from the superposition method was nearly equal to the one simply estimated from the method with the autocorrelation coefficient or frequency analysis of the vibration waveform in single-shot blasting [18]. Azizabadi et al. simulated the surface vibration generated by blasting in the stability assessment of the rock slope of an open-pit mine through the vibration measurement data of a single blasting hole. The simulated production blast seismograms were then adopted as input to predict the time histories of particle velocity in the blast vibrations on the mine wall by using the universal distinct element code. The simulated time histories of particle velocity were consistent with the measured data [19]. Navarro Torres et al. collected data, which were processed with multiple regression techniques, to obtain the blasting vibration attenuation law and predict the levels of blasting-induced vibrations for the locality under study. They had knowledge of only the maximum explosive charge per delay and the distance to the blasting point. The Brazilian and international admissibility standards of blasting-induced vibration, the minimum distance between the mine and the community, and the constants obtained from the regression were used to establish the maximum explosive charge per delay for an acceptable ground vibration level that would not cause structural damage and human discomfort [20]. For the cylindrical charge, many scholars combined dynamic caustics, super dynamic strain testing, and numerical analysis methods to study the explosion stress and strain field of the cylindrical charge and the evolution law of the local stress field at the tip of the explosion crack [21–24]. Some scholars have also conducted intensive research on the different charge structures of columnar drug packs. Through different positions and proportions of air deck, the action time in the cylindrical charge hole is extended to improve the utilization rate of explosives and reduce the blasting vibration [25–29].

At present, five technical problems must be solved for the expansion of the 24-m-high bench in Barun open-pit mine. First, the perforation depth of ordinary roller drills does not exceed 20 m and thus cannot meet the requirements of a 24-m-high bench and large diameter drilling. Second, limited by the slope of the bench, the height of the bench increases, and the resistance line of the front row is doubled. Effectively breaking and moving the rock at the bottom of the hole are greatly challenging. Third, if the high-bench deep hole adopts a continuous charge structure, then the unit consumption of explosives under the same hole layout condition is higher than that of ordinary bench blasting, and the cost will increase. Fourth, the increase of the height and charge of the bench will inevitably lead to an increase of blasting vibration in the middle and far areas. Fifth, the current dynamic response of the rock medium under the blasting load of the spherical or cylindrical charge will produce huge errors in the design of loosening blasting with a high bench and a large spacing parameter. In this study, the analysis of the physical mechanism of the stress wave attenuation in the rock indicates that the cylindrical charge is equivalent to several spherical charges. Considering the pressure attenuation, reflection, transmission, and superposition of the spherical charge after the equivalence, a double exponential function correction equation of the stress wave attenuation is obtained based on the Mises strength criterion. The stress of any point in the rock medium with various spacing parameter is obtained by calculation. ANSYS/LS-DYNA is used to simulate and study the stress distribution of a 24-m-high bench with various spacing parameters. Meanwhile, the accuracy of the correction equation is verified. The parameters of the high-bench blasting with good effect and low cost are determined. Finally, a field test is conducted to analyze the blasting effect.

2. Dynamic Response and Failure Criterion of Rock in Column Explosion Load

2.1. Stress Field Characteristics of Spherical Charge. When the charge blast hole is detonated, the explosive will explode to produce high-pressure gas, impacting the wall and propagating a strong pressure wave outward into the rock medium [30]. According to the degree of damage to the surrounding rocks, three zones are formed on the rocks: the cavity, broken, and elastic zones. The elastic zone is divided into the crack and vibration zones (as shown in Figure 1). Therefore, the blasting seismic wave is the propagation of the wave filtered through the broken and radial crack zones. The cavity wall propagates under the action of the continuous expansion and contraction of the explosive gas. This process involves the interaction between the high-pressure expansion of explosive detonation products and the rock mass, the constitutive characteristics of the rock mass state of the fracture zone and the fracture zone, the size of the failure zone, and the stress time history at the interface of the failure and elastic vibration zones. The study of this issue is the most basic and important in the study of blasting seismic wave effects.

The known characteristics of the stress field of the spherical charge indicate that the law of stress attenuation is proportional to the explosive quantity and inversely proportional to the distance [31]. The energy density (E) of the spherical charge decays according to the cubic relationship of the expansion path (R). Moreover, the explosive mass is only a representation of energy, so the energy density attenuation formula of the spherical charge can be abbreviated as

$$E = k\frac{f(q)}{R^3} = k\frac{(4/3)\pi r_b^3 \rho q}{R^3}, \tag{1}$$

where q is the explosive heat, r is the radius of the spherical charge, ρ is the explosive density, R is the energy field radius of the spherical charge, and k is the correlation coefficient of energy attenuation.

The local field characteristic theorem of waves points out that the reflection or transmission of the incident wavefront with arbitrary shapes at any point on the curved interface is the same as that of plane waves [32, 33]. Therefore, the transmission and reflection problems of arbitrary incident wavefront on the curved interface can be simplified as plane wave problems. The calculation method for the initial pressure of the wall of the borehole with a coupled charge is generally in accordance with the following equation:

$$P_0 = \frac{\rho_e D_e^2}{k+1}, \tag{2}$$

where ρ_e is the explosive density, D_e is the explosive velocity, $\rho_e D_e$ is the explosive wave impedance, and k is the adiabatic index, which is the slope of the pressure and volume curve when the entropy value is constant, and its value is related to explosive density and explosive heat. Jones proposed that

$$k = \frac{(1+a) + [2(1+a) - 1] \times (1.33\rho_e/G)}{1 + (1.33\rho_e/G)}, \tag{3}$$

where $(1+a)$ is the ratio of the specific heat of the detonation gas product in an ideal state and G is the part of the

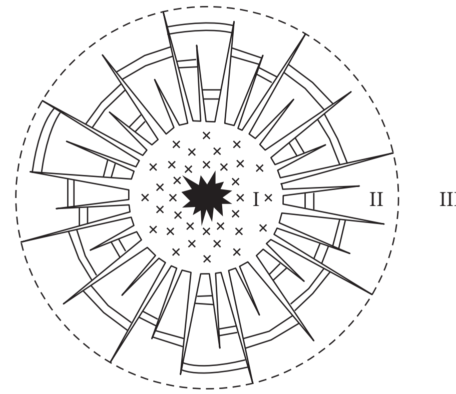

Figure 1: Blasting zones partitioned in the rock, indicating the (I) crush zone, (II) fracture zone, and (III) elastic vibration zone.

detonation heat of the detonation gas product. When the explosive density is very small, the adiabatic index can be $k = 4/3$. Chen et al. [34] believed that the adiabatic index is only related to the density of explosives and expressed their relationship as follows:

$$k = 1.9 + 0.6\rho_e. \tag{4}$$

For most explosives, $k = 3$ is generally approximated.

Some scholars provided a double exponential function describing the stress wave attenuation with time excited by the spherical charge [35–37]:

$$P(t) = P_0\left(e^{-At} - e^{-Bt}\right),$$

$$\begin{cases} \omega = \dfrac{2\sqrt{2}\,c}{r_0}, \\[2ex] A = \dfrac{nw}{\sqrt{2}}, \\[2ex] B = \dfrac{mw}{\sqrt{2}}, \end{cases} \tag{5}$$

where ω is the angular frequency, c is the propagational velocity of the longitudinal wave, and r_0 is the radius of the cavity.

$$\begin{aligned} \psi = &-\frac{(r_0 p_0/\rho l)}{((\omega/\sqrt{2}) - A)^2 + \omega^2} e^{-At} + \frac{(r_0 p_0/\rho l)}{((\omega/\sqrt{2}) - B)^2 + \omega^2} e^{-Bt} \\ &+ \frac{(r_0 p_0/\rho l)}{((\omega/\sqrt{2}) - A)^2 + \omega^2}\left[\left(\frac{1}{\sqrt{2}} - \frac{A}{\omega}\right)\sin\omega t + \cos\omega t\right] e^{-\omega t\sqrt{2}} \\ &- \frac{(r_0 p_0/\rho l)}{((\omega/\sqrt{2}) - B)^2 + \omega^2}\left[\left(\frac{1}{\sqrt{2}} - \frac{B}{\omega}\right)\sin\omega t + \cos\omega t\right] e^{-\omega t\sqrt{2}}. \end{aligned} \tag{6}$$

From the second-order partial derivative of the displacement potential function, the particle strain potential function is as follows:

$$\begin{aligned}
\varepsilon_l = \frac{\partial^2 \psi}{\partial l^2} = \frac{9p_0}{4\rho c^2}\left(\frac{l}{r_0}\right)\Bigg\{ &-\left[2\left(\frac{l}{r_0}\right)^2 - \frac{4n}{3}\frac{l}{r_0} + \frac{4n^2}{9}\right]\frac{e^{-n\omega t\sqrt{2}}}{3-2n+n^2} \\
&+ \frac{e^{-\omega t\sqrt{2}}}{\sqrt{2}\sqrt{3-2n+n^2}}\left[2\left(\frac{l}{r_0}\right)^2 \sin(\omega t+\alpha) - \frac{4\sqrt{3}}{3}\left(\frac{l}{r_0}\right)\sin(\omega t+\alpha-\gamma) + \frac{4}{3}\sin(\omega t+\alpha-2\gamma)\right] \\
&+ \left[2\left(\frac{l}{r_0}\right)^2 - \frac{4m}{3}\frac{l}{r_0} + \frac{4m^2}{9}\right]\frac{e^{-m\omega t\sqrt{2}}}{3-2m+m^2} - \frac{e^{-\omega t\sqrt{2}}}{\sqrt{2}\sqrt{3-2m+m^2}} \\
&\cdot \left[2\left(\frac{l}{r_0}\right)^2 \sin(\omega t+\beta) - \frac{4\sqrt{3}}{3}\left(\frac{l}{r_0}\right)\sin(\omega t+\beta-\gamma) + \frac{4}{3}\sin(\omega t+\beta-2\gamma)\right]\Bigg\}.
\end{aligned} \tag{7}$$

The symbols are listed in Table 1. Assuming that the rock medium obeys Hooke's law, the radial stress at any point in the medium can be obtained.

3. Blasting Load of Cylindrical Charge and Rock Dynamic Response

When the conditions are consistent, according to the quasi-static model of the spherical charge, Starfield approximates that the cylindrical charge is composed of multiple spherical charge stacks. The diameter of the spherical charge should be as near as possible or equal to the diameter of the cylindrical, as shown in Figure 2.

Each spherical charge has a stress effect on a certain point in the rock medium during the entire time of the positive pressure. Assuming that the stress wave of the spherical charge reaches the specified point when the stress peak occurs, the decay time difference can be obtained:

$$f(t,\xi) = t - t_0 - \frac{2r_0(\xi-1)}{D}, \quad \xi = (i,j,k), \tag{8}$$

where i, j, and k are the spherical number in various cylindrical charge, ξ is the distance from the spherical charge to the detonation point, t is the starting time from the detonation point, t_0 is the detonation delay time of the cylindrical charge, and D is the explosive velocity. According to the stress attenuation in the medium after spherical charge blasting, the radial stress at any point is calculated. The transmitted shock waves in the rock continue to propagate outward and finally become stress waves. For the force state of the element at any point in the rock as a plane strain problem, the tangential stress at any point in the rock can be obtained:

$$\begin{aligned}
\sigma_r &= F[P(t), f(t,\xi)] \\
&= \sum_{i=1}^{i} P[f(t), i] + \sum_{j=1}^{j} P[f(t), j] + \sum_{k=1}^{k} P[f(t), k],
\end{aligned} \tag{9}$$

$$\sigma_\theta = -b\sigma_r, \tag{10}$$

$$\sigma_z = \mu_d(1-b)\sigma_r, \tag{11}$$

where b is the coefficient of lateral, σ_r and σ_θ are the radial and tangential stresses in the rock, respectively, and σ_z is the normal surface stress formed by σ_r and σ_θ.

3.1. Stress State and Strength Failure Criterion of Rock Mass in Blasting Loading. The stress tensor at any point in the rock is usually described by six independent stress components or three principle stresses acting on mutually perpendicular planes. The magnitude and direction of the stress tensor component are different for different coordinate systems, but the stress tensor and stress deflection invariants at this point will not change with the coordinate system. Therefore, the invariants of stress and deviatoric stress tensor play an important role in strength theory. For plastic media, the deformation state in the deformation zone must be studied, that is, the initial yield and plastic states during the deformation process when a point is in the elastic state. Usually, the stress tensor is divided into two parts: one part is the spherical stress tensor or the hydrostatic stress tensor, and the other part is the deviatoric stress tensor. Therefore, when the stresses are equal in all directions, it is equivalent to hydrostatic pressure and does not produce plastic deformation. Therefore, separating the same stress in all directions from the stress tensor is convenient for studying plastic deformation:

$$\begin{gathered}
\sigma_{ij} = \sigma_m \delta_{ij} + s_{ij}, \\
\delta_{ij} = \begin{cases} 1, & i = j, \\ 0, & i \neq j, \end{cases} \\
\begin{cases}
J_1 = s_x + s_y + s_z = \sigma_x + \sigma_y + \sigma_z - 3\sigma_m, \\
J_2 = -\left(s_x s_y + s_y s_z + s_z s_x\right) + \tau_{xy}^2 + \tau_{yz}^2 + \tau_{zx}^2 \\
\quad = \dfrac{1}{6}\left[\left(\sigma_x - \sigma_y\right)^2 + \left(\sigma_y - \sigma_z\right)^2 + \left(\sigma_z - \sigma_x\right)^2 + 6\left(\tau_{xy}^2 + \tau_{yz}^2 + \tau_{zx}^2\right)\right], \\
J_3 = s_x s_y s_z + 2\tau_{xy}\tau_{yz}\tau_{zx} - s_z\tau_{yz}^2 - s_y\tau_{zx}^2 - s_z\tau_{xy}^2,
\end{cases}
\end{gathered} \tag{12}$$

where δ_{ij} is the Kronecker symbol, $\sigma_m\delta_{ij}$ is the stress sphere tensor, which represents the equal normal stress in three

Table 1: List of symbols.

r_0 = Radius of cavity
c = propagational velocity of longitudinal wave
e = base of the natural system of logarithms
m = constant (when $t = 0$, $m = 0$)
n = constant (when $t = 0$, $n = 0$)
p = variable pressure
p_0 = Constant pressure
t = time
l = radial distance from the center of the cavity
A = constant
B = constant
α = phase angle
β = phase angle
γ = phase angle
ε_l = Radial strain
ψ = Displacement potential function

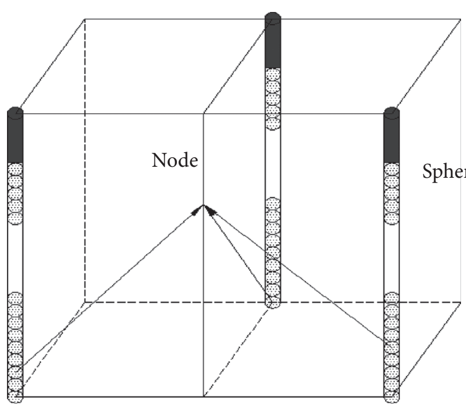

Figure 2: Cylindrical charge as near as possible or equal to the spherical charge.

directions, s_{ij} is the stress deflection tensor, and J_1, J_2, and J_3 represent the first, second, and third invariants of the stress deviator, respectively. When the x, y, and z axis directions coincide with the main axis,

$$\begin{cases} J_1 = 0, \\ J_2 = \frac{1}{6}\left[(\sigma_1 - \sigma_2)^2 + (\sigma_2 - \sigma_3)^2 + (\sigma_3 - \sigma_1)^2\right], \\ J_3 = s_1 s_2 s_3. \end{cases} \tag{13}$$

For any point in space, the size of the deviatoric stress tensor part vector NP can be represented by r, and R is the size of the deviatoric stress tensor length when yielding occurs (as shown in Figure 3). When $r < R$, point P is located inside the Mises yield cylinder and is in an elastic state; when $r = R$, point P is located on the Mises yield cylinder and is yielding; when $r > R$, point P is located outside the Mises yield cylinder and is in a plastic state phase:

$$\sigma_i = \sqrt{\frac{1}{3}\left[(\sigma_r - \sigma_\theta)^2 + (\sigma_\theta - \sigma_z)^2 + (\sigma_z - \sigma_r)^2\right]} = \sqrt{2J_2}. \tag{14}$$

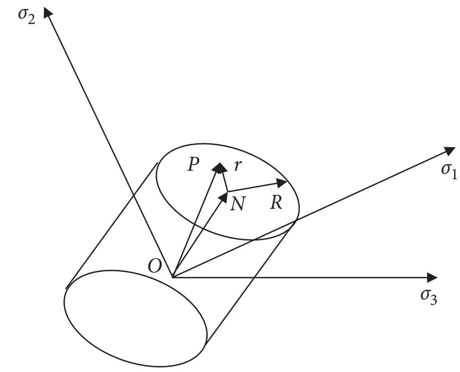

Figure 3: Mises yield criterion in the principle stress space.

In the crushing area, $\sigma_i \geq \sigma_{cd}$; in the fracture area, $\sigma_i \geq \sigma_{td}$; σ_{cd} is the dynamic compressive strength of the rock; σ_{td} is the dynamic tensile strength of the rock.

Equations (9)–(11) can be used to obtain the stress of a point in the medium in different directions (as shown in Figure 4). By substituting it into formula (14), the effective stress at any point can be obtained (as shown in Figure 5), and then, the effective stress attenuation with distance can be obtained (as shown in Figure 6).

4. Numerical Simulation Research of Large Spacing Parameter for Loosening Blasting with 24-m-High Bench in Barun Open-Pit Mine

4.1. Engineering Overview. The 1120 horizontal loosening blasting project in Barun open-pit mine was selected as the test area. Three hole-blasting models with spacing parameter of 13 m × 6 m and 15 m × 5.5 m (concentration factor 2.73) were established. According to the Saint–Venant principle, the design parameters of the high-bench model are as follows: the total height is 40 m, the height of the bench is 24 m, the bottom square is 40 m × 40 m, the top square is 19 m × 40 m, the extra depth is 2 m, and the resistance line is 14.19 m. The model structure is shown in Figure 7. The front and back of the bench model are defined as reflective boundaries, the slope and ground surfaces are defined as free boundaries, and the other surfaces in contact with air are defined as nonreflective boundaries. The detonation times of the first, second, and third holes are 0, 42, and 142 ms, respectively, and two detonation points in each hole detonate at the same time. The multimaterial ALE algorithm is used on the results of explosives and air, the Lagrange algorithm is used on the rocks and the stemming, and the fluid-solid coupling algorithm is used to reflect the stress transfer between explosives, air, and rocks.

4.2. Establishment of the Numerical Model. Many methods can accurately describe the pressure change process during charge detonation in numerical simulation. The basic principle is to describe the dynamic expansion of the entire detonation chamber by combining the detonation research results of explosives with the state equation of detonation

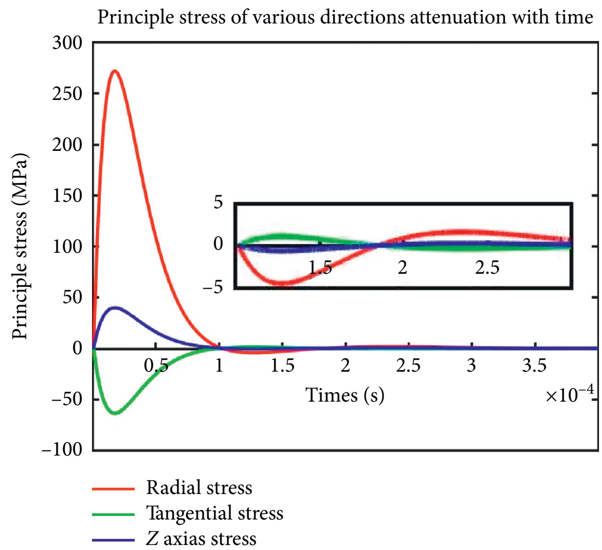

FIGURE 4: Principle stress of various direction attenuations with time.

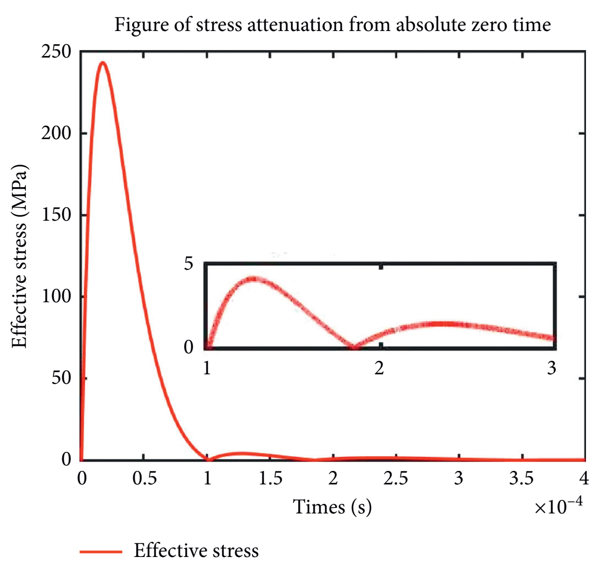

FIGURE 5: Effective stress attenuation from absolute zero time.

gas. LS-DYNA program can directly simulate the detonation process of high-energy explosives. At any moment, the explosive pressure on the surrounding rock is as follows:

$$P = FP_{eos}(V, E),$$

$$F = \begin{cases} \dfrac{2(t - t_1)DA_{emax}}{3v_e}, & (t > t_1), \\ 0, & (t \le t_1), \end{cases} \tag{15}$$

where P is the explosion pressure, F is the chemical energy release rate of the explosive, V is the explosive detonation velocity, t and t_1 are the initiation times of the current time and inside the explosive, respectively, A_{emax} is the maximum cross-sectional area of the explosive unit, and v_e is the unit volume of explosive.

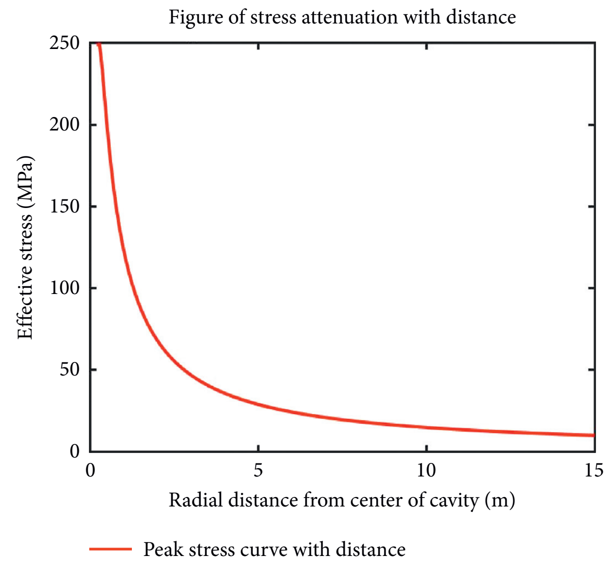

FIGURE 6: Effective stress attenuation with distance.

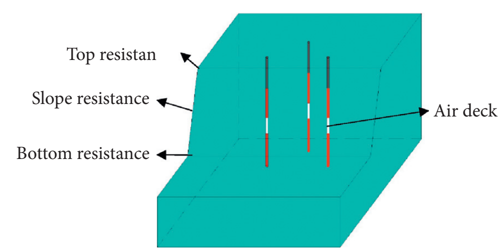

FIGURE 7: Schematic of blast holes location and charge structure.

In this study, the high-performance explosive model (∗Mat_High_Explosive_Burn) and the JWL equation are adopted to simulate blasting. The parameters are shown in Table 2.

$$P_{eos} = A\left(1 - \frac{\omega}{R_1 V}\right)e^{-R_1 V} + B\left(1 - \frac{\omega}{R_2 V}\right)e^{-R_2 V} + \frac{\omega E_0}{V}, \tag{16}$$

where P_{eos} is the pressure determined by the JWL equation of the state, V is the relative volume, E_0 is the initial specific internal energy, and A, B, R_1, R_2, and ω are the five independent physical constants that describe the JWL equation.

The parameters of the air model (*Mat_Null) and the state equation (*Eos_Linear_Polynomial) are shown in Table 3. The density of air is 1.225 kg/m^3. The pressure is simulated by a linear polynomial equation of state (*Eos_Linear_Polynomial). The equation is expressed as follows:

$$\begin{cases} P_{poly} = C_0 + C_1\mu + C_2\mu^2 + C_3\mu^3 + \left(C_4 + C_5\mu + C_6\mu^2\right)E, \\ \mu = \dfrac{1}{V} - 1, \end{cases} \tag{17}$$

where C_0–C_6 are constants, μ is the volume ratio, and E is the ratio of internal energy to initial volume.

Table 2: Parameters of explosive and JWL equation.

Parameters	ρ (kg/m^3)	D (m/s)	P_{CJ} (GPa)	A (GPa)	B (GPa)	R_1	R_2	ω	E_0 (GPa)	V_0
Value	1250	3600	5.4	374.0	3.23	5.80	1.56	0.57	2.6728	1.0

Table 3: Parameters of the air model and the state equation.

Parameters	ρ_0	E_0	v_o	C_0~C_3	C_4	C_5	C_6
Value	1.225	2.5E5	1.0	0	0.4	0.4	0

Table 4: Parameters of the rock mass.

Parameters	ρ (kg/m^3)	σ_t (MPa)	σ_c (MPa)	E (GPa)	μ
Dolomite	3060	14	66.76	45.96	0.376

The plastic model (*Mat_Plastic_Kinematic) is adopted for the rock and the blockage (parameters are shown in Table 4). The Eulerian algorithm is used for the explosive, air, and blockage material models. The Lagrange algorithm is applied to the rock model. If the fluid-structure interaction algorithm is applied, no element distortion will occur. Given this advantage, the algorithm has been widely used in engineering numerical simulation with large deformation and high strain rate. Hence, the multimaterial fluid-structure interaction algorithm can be applied to deal with the interaction process of detonation products and the surrounding rock media. The maximum unit side length in the divided model mesh is 0.25 m, and the parts around blast holes are encrypted.

5. Comparison Analysis of Numerical Simulation Results and Theoretical Calculation

The boundary of the fissure circle formed after the cylindrical charge is detonated is determined by the dynamic tensile strength of the rock. According to previous research on the rock tensile strength of the main ore rocks in Barun open-pit mine, the dynamic tensile strength of the dolomite is taken as $\sigma = 14.0$ MPa. Therefore, if the effective stress peak value of each element in the model reaches or exceeds the dynamic tensile strength of this dolomite, then the rock represented by this element will be damaged. Otherwise, the rock will not be damaged to form a fractured ring. The center planes of the two holes on the bench slope are sequentially selected from the top to the bottom, and the effective stress-time diagram is drawn. Furthermore, the monitoring points are uniformly selected at the resistance line at the bottom of the bench slope, and the effective stress-time diagram is drawn.

The middle point of the front row of holes and the position of the rear row of holes are selected as the cross-section, and the maximum effective stress is analyzed. The effective stress of the rock mass can reflect rock fragmentation. When hole 1 detonates for 1.99 ms, the effective stress in the middle of the section can reach 81.5 MPa, and the effective stress at the slope resistance line can reach up to 38.78 MPa. When the 43.39 ms hole 2 detonates at 1.39 ms, the stress wavefronts between the two holes are superimposed on each other, and the synergistic effect is obvious. When the 144 ms hole 3 detonates at 2 ms, the back row hole explosion stress wavefront reaches the front row hole center. The line position further plays the role of breaking the rock and pushing the rock forward.

The comparison of the maximum effective stress at the top observation point of the two spacing parameter indicates that the stress values present a trend of decreasing first and then increasing. The maximum effective stress of the 13 m × 6 m section is larger than that of the 15 m × 5.5 m section, as shown in Figures 8 and 9. The stress peak near the middle of the front holes indicates that the blasting action of the front row of holes sufficiently broke the rock between the two holes, creating a good free surface for the rear row of holes and achieving a good blasting effect.

The maximum stress of the slope observation point of the two spacing parameters arrangement methods increases first and then decreases. As shown in Figures 10 and 11, the maximum stress at the 13 m × 6 m spacing parameter observation point is far greater than the compressive strength of the rock, and the blasting energy is unevenly distributed along the bench slope, which can easily cause harmful effects, such as flying rocks. In comparison, the maximum stress at the observation point of the 15 m × 5.5 m spacing parameter is greater than the dynamic tensile strength of the rock, which can achieve the effect of rock breaking. Meanwhile, due to the existence of air gap, the rock breaking time is prolonged, and the energy distribution is more even. It not only will not cause the waste of blasting energy but also will not cause harmful effects, such as flying rocks and excessive vibration.

As shown in Figures 12 and 13, through numerical simulation, the maximum effective stress (22.6 MPa) at the bottom resistance line observation point of the 15 m × 5.5 m spacing parameter is much smaller than the maximum effective stress (29.58 MPa) at the 13 m × 6 m spacing parameter. Meanwhile, the existence of air gap equalizes the detonation gas pressure in the hole, and the stress at the 15 m × 5.5 m spacing parameter observation point is more uniform, which can achieve the rock breaking effect while avoiding the bedrock exit.

Different combinations of spacing parameter will have different effects on the blasting effect. According to the maximum effective stress analysis of the simulated results of different section monitoring points and the comparison of the theoretical calculation values, as shown in Figures 14–16, the three sections that meet the rock crushing requirements are selected for the field test. The evaluation of numerical simulation results of various spacing parameter indicates that the 15 m × 5.5 m combination comprehensive evaluation effect is the best.

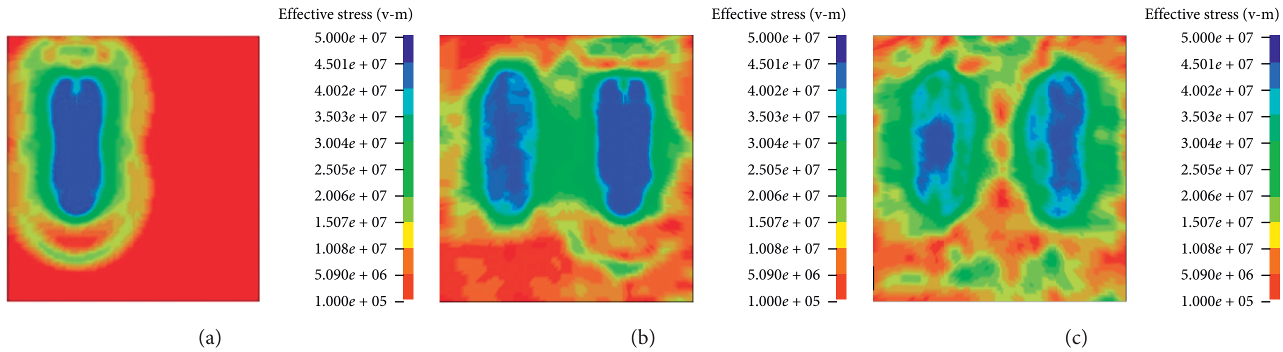

FIGURE 8: 13 m × 6 m effective stress of the section between the front holes at different times. (a) $t = 1.99$ ms. (b) $t = 43.49$ ms. (c) $t = 144.00$ ms.

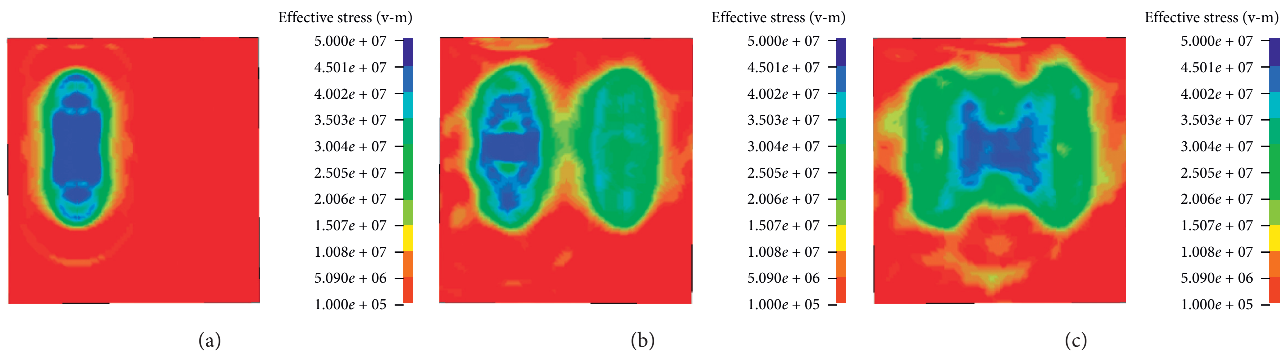

FIGURE 9: 15 m × 5.5 m effective stress of the section between the front holes at different times. (a) $t = 1.99$ ms. (b) $t = 43.49$ ms. (c) $t = 144.00$ ms.

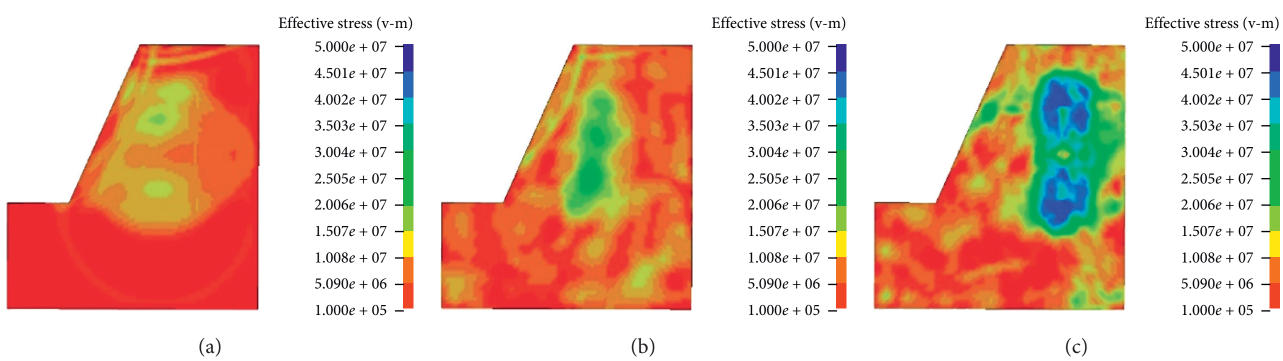

FIGURE 10: 13 m × 6 m effective stress of the section between the front holes at different times. (a) $t = 1.99$ ms. (b) $t = 43.49$ ms. (c) $t = 144.00$ ms.

5.1. Field Test. The air deck charge structure and the large spacing parameter of the hole layout result in insufficient bench explosion energy and easily produce large blocks. During the blasting process, the resistance line at the bottom of the bench is extremely large, and the rock is difficult to break. Thus, high-bench blasting is more likely to produce the foundation than ordinary bench blasting. Through the improvement of Barun open-pit mine's drilling rig, the drilling depth can reach 26 m to 27 m, which meets the requirements of 24-m-high bench drilling. At present, the large domestic air deck charge structure and the method of arranging holes with large spacing parameter have not been adopted in noncoal mines. Barun open-pit mine has carried out high-bench blasting tests and achieved significant results, but its use is still difficult to promote in mines. After improvement, the field test blasting area is designed to use vertical drilling for the 24-m-high bench blasting design. The drilling rig type is a YZ-55B roller drill with a drill bit diameter of 310 mm and a slope angle of 78°. The depth of the hole is 26 m, including the super deep is 2 m, the blockage is 7 m, the air deck is 7 m, and the remaining 12 m are used for charging. Considering the

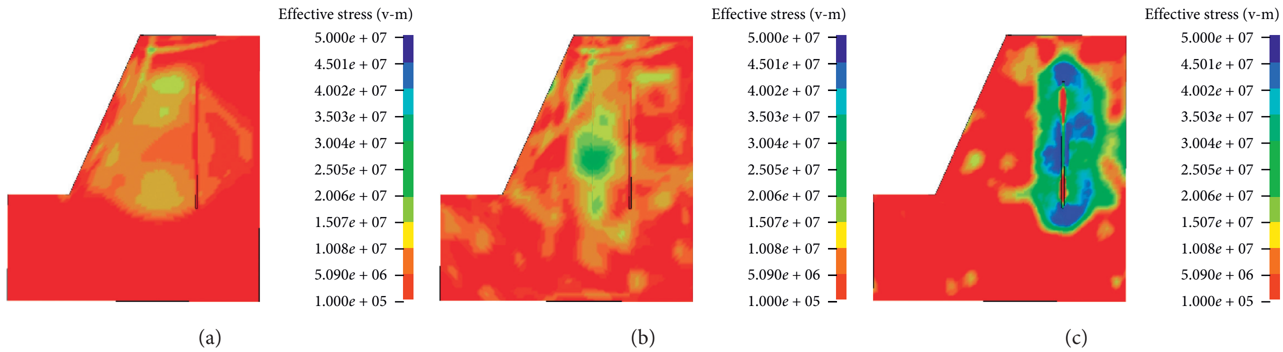

FIGURE 11: 15 m × 5.5 m effective stress of the section between the front holes at different times. (a) t = 1.99 ms (b) $t = 43.49$ ms (c) $t = 144.00$ ms.

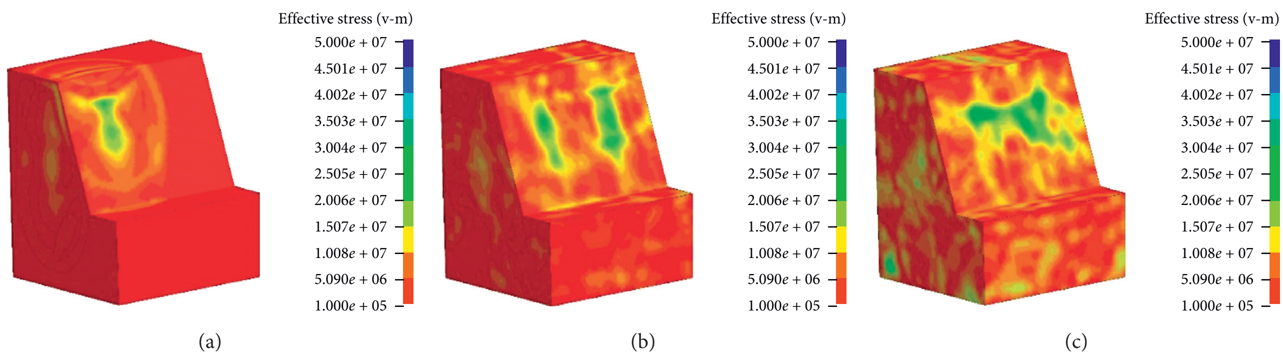

FIGURE 12: 13 m × 6 m effective stress of the section between the front holes at different times. (a) $t = 1.99$ ms. (b) $t = 43.49$ ms. (c) $t = 144.00$ ms.

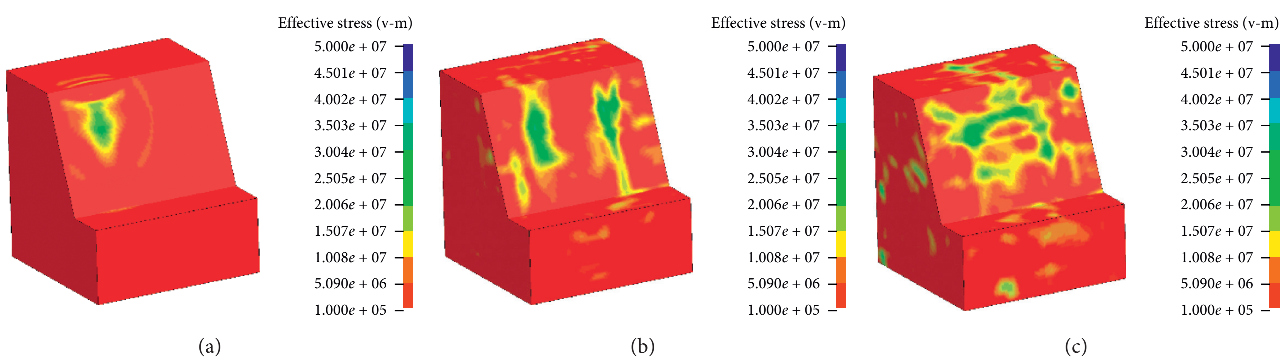

FIGURE 13: 15 m × 5.5 m effective stress of the section between the front holes at different times. (a) $t = 1.99$ ms. (b) $t = 43.49$ ms. (c) $t = 144.00$ ms.

construction problems and the pressure bearing capacity of the air spacer and overcoming the bottom resistance line, the air spacer is arranged in the middle of the blast hole. Using a large spacing parameter, the spacing is 15 m, and the row spacing is 5.5 m. The hole-by-hole initiation method has a short interval of 25 ms. The main rock at the site is dolomite, and the other rock composition is relatively small. The simulation is performed under a single dolomite condition. This is the limitation of the simulation. Although some differences from the site exist, it can represent most of the site conditions and must be verified by experiments. The surface rock on-site is quaternary, with low hardness, small thickness, and uneven distribution, so the impact on blasting can be ignored.

According to the existing shovel loading equipment in the mining area, the statistical analysis of the rock mass after blasting shows that the large lump rate in the experimental blasting area is only 0.01%, which meets the requirements of

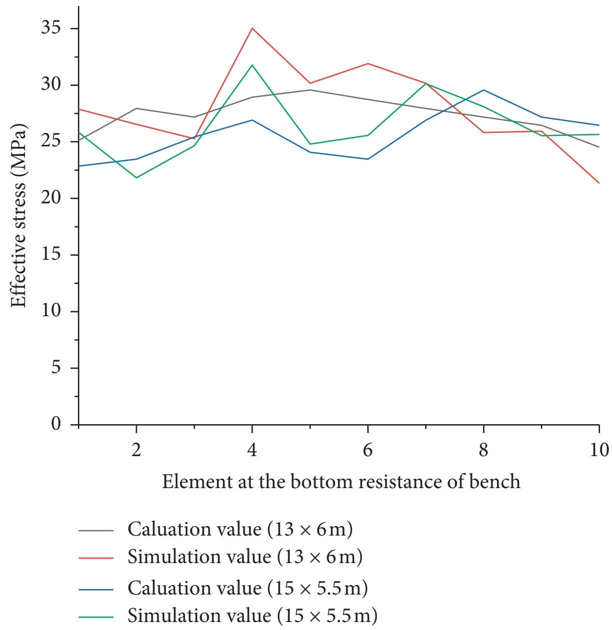

Figure 14: Effective stress of the section at the bottom resistance of bench.

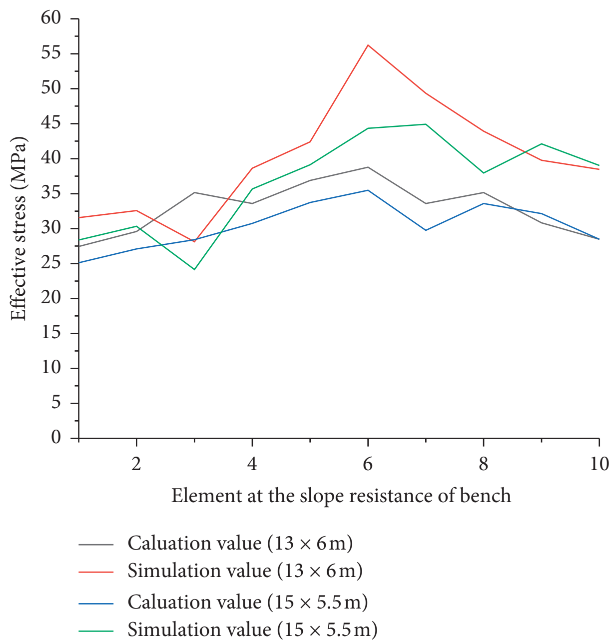

Figure 15: Effective stress of the section at the slope resistance of bench.

the shovel (as shown in Figure 17). The TC-4850 blasting monitoring instrument was used to test the vibration of the field test explosion zone, which was compared with the conventional bench blasting vibration (Table 5). Analysis indicates that although the single-hole charge of high-bench blasting is greater than that of conventional blasting, the air deck weakens the peak pressure, so the blasting vibration increases slightly, and it meets safety requirements.

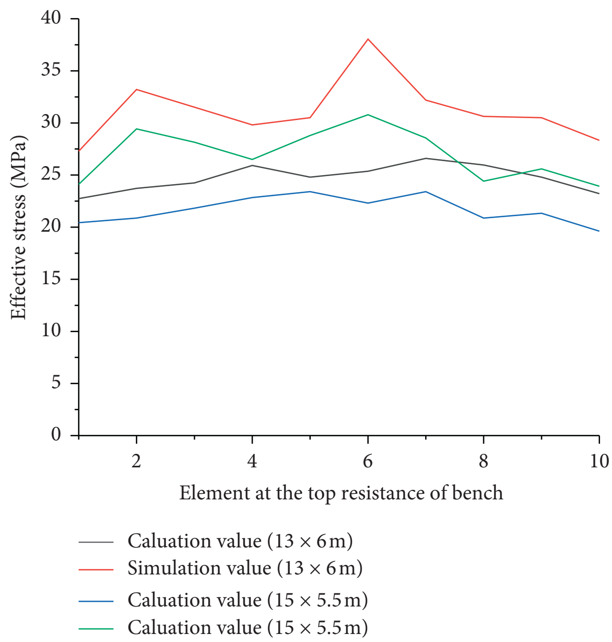

Figure 16: Effective stress of the section at the top resistance of bench.

Figure 17: Effective stress of the section between the front holes at different times.

Table 5: Comparison of blasting vibration speed.

Blasting area	Direction	Maximum vibration speed (cm/s)
1460 horizontal conventional blasting zone	X	−5.551
	Y	−3.707
	Z	7.032
1120 horizontal loosing blasting zone	X	7.322
	Y	−5.835
	Z	8.763

6. Conclusions

(1) The theoretical calculations and the numerical simulation stress cloud diagrams were compared to analyze the rock stress state. Not only the distribution of holes with large spacing parameter has a good synergy effect between the holes but also the front row of holes can also provide a better facing surface for the rear row of holes to improve the blasting effect.

(2) The numerical simulation value has a larger stress value on the slope, and the coverage area on the top of the bench is larger than the theoretical calculation value, indicating that when the air deck is in the middle of the blast hole, the theoretical calculation value ignores the reflection of the stress after reaching the free surface. The stress value at the observation point has less dispersion. Combined with the explosive pile shape at the scene, the air deck charge effect in the middle of the blast hole is better. The application of air deck equalizes the detonation gas pressure in the hole and prolongs the rock breaking time, which not only reduce the number of

explosives but also improve the crushing effect of the bottom rock.

(3) The theoretical calculation is basically consistent with the field test results. The application of loosening blasting technology with a large spacing parameter of 15 m × 5.5 m improves the quality of loosening blasting. This technology can reduce the bulk rate and the appearance of roots. It avoids harmful effects, such as flying rocks, reduces the blasting cost by approximately 20%, and achieves good results in the 1120 m horizontal blasting zone of Barun open-pit mine.

(4) The error between the theoretical and simulated values is small. Compared with the numerical calculation, the stress wave attenuation double exponential function correction equation based on the Mises strength criterion can be popularized in field production applications. The equation can be easily used by all kinds of technicians, which is beneficial to improving blasting efficiency and reducing the consumption of explosives.

Data Availability

The data included in this study are available from the corresponding author upon request.

Conflicts of Interest

The authors declare that they have no conflicts of interest.

Acknowledgments

The authors would like to thank the Barun Mining Co. Ltd. of Baotou Steel Group.

References

[1] Z. Q. Liu, D. S. Wang, F. Cui, X. D. Xu, and D. Lan, "Experimental research on 24 m high bench blasting technique in Barun mine," *Metal Mine*, vol. 6, pp. 68–71, 2019.

[2] L. Y. Qi, D. S. Wang, Z. Q. Liu, F. Cui, X. D. Xu, and J. X. Guo, "Prediction of pre-split blasting effect based on BP neural network," *Metal Mine*, vol. 7, pp. 65–69, 2019.

[3] G. L. Wang, D. S. Wang, W. Q. Lu, H. P. Qiao, F. Li, and H. Chen, "Study on big dense coefficient blasting technology of soft and hard stratigraphic overlay and stratified development rock mass," *Engineering Blasting*, vol. 25, no. 2, pp. 26–30, 2019.

[4] X. H. Zhang, W. Q. Lu, H. P. Qiao, P. Cheng, and F. Li, "Study and application of loose blasting technology with large-density coefficient for layered rock mass," *Mining Research and Development*, vol. 39, no. 12, pp. 136–139, 2019.

[5] J. Peng, F. Zhang, C. Du, and X. Yang, "Effects of confining pressure on crater blasting in rock-like materials under electric explosion load," *International Journal of Impact Engineering*, vol. 139, 2020.

[6] M. Chen, W. B. Lu, C. B. Zhou, D. Q. Shu, and H. T. Xu, "Rock slope stability under blasting vibration based on equivalent acceleration," *Explosion and Shock Waves*, vol. 31, no. 5, pp. 475–480, 2011.

[7] H. B. Xia, Y. Xu, Q. Zong, and J. G. Fu, "Observation study of fissure rock damage range under blasting load," *Rock and Soil Mechanics*, vol. 4, pp. 795–798, 2007.

[8] X. Zhang and D. Q. Shu, "Numerical simulation and mechanism analysis of rock fragmentation of wide hole-distance blasting," *Blasting*, vol. 29, no. 4, pp. 42–45, 2012.

[9] Q. Zong and D. J. Meng, "Influence of different kinds of hole charging structure on explosion energy transmission," *Chinese Journal of Rock Mechanics and Engineering*, vol. 22, no. 4, pp. 641–645, 2003.

[10] Q. Li, H. J. Wang, and R. S. Yang, "Experimental investigation on fracture process of multi-hole bench blasting," *Journal of China Coal Society*, vol. 5, pp. 34–37, 2005.

[11] V. Balakrishnan, M. Pradhan, and P. Y. Dhekne, "Investigating rock fragmentation in distributed spherical air-gap blasting technique," *Powder Technology*, vol. 362, pp. 101–110, 2020.

[12] D. P. Blair, "Approximate models of blast vibration in non-isotropic rock masses," *International Journal of Rock Mechanics and Mining Sciences*, vol. 128, Article ID 104245, 2020.

[13] A. K. Chakraborty, J. L. Jethwa, and A. G. Paithankar, "Effects of joint orientation and rock mass quality on tunnel blasting," *Engineering Geology*, vol. 37, no. 3-4, pp. 247–262, 1994.

[14] S. Gómez, J. A. Sanchidrián, and P. Segarra, "Near-field vibration from blasting and rock damage prediction with a full-field solution," *International Journal of Rock Mechanics and Mining Sciences*, vol. 134, Article ID 104357, 2020.

[15] A. K. Raina, V. M. S. R. Murthy, and A. K. Soni, "Estimating flyrock distance in bench blasting through blast induced pressure measurements in rock," *International Journal of Rock Mechanics and Mining Sciences*, vol. 76, pp. 209–216, 2015.

[16] B. K. Singh, D. Mondal, M. Shahid, A. Saxena, and P. N. S. Roy, "Application of digital image analysis for monitoring the behavior of factors that control the rock fragmentation in opencast bench blasting: a case study conducted over four opencast coal mines of the Talcher coalfields, India," *Journal of Sustainable Mining*, vol. 18, no. 4, pp. 247–256, 2019.

[17] D. W. Zhong, L. He, P. Cao, and X. W. Huang, "Experimental study of reducing vibration intensity based on controlled blasting with precise time," *Journal of China Coal Society*, vol. 40, no. S1, pp. 107–112, 2015.

[18] K. Iwano, K. Hashiba, J. Nagae, and K. Fukui, "Reduction of tunnel blasting induced ground vibrations using advanced electronic detonators," *Tunnelling and Underground Space Technology*, vol. 105, 2020.

[19] H. R. M. Azizabadi, H. Mansouri, and O. Fouché, "Coupling of two methods, waveform superposition and numerical, to model blast vibration effect on slope stability in jointed rock masses," *Computers and Geotechnics*, vol. 61, pp. 42–49, 2014.

[20] V. F. Navarro Torres, L. G. C. Silveira, P. F. T. Lopes, and H. M. de Lima, "Assessing and controlling of bench blasting-induced vibrations to minimize impacts to a neighboring community," *Journal of Cleaner Production*, vol. 187, pp. 514–524, 2018.

[21] C. Ding, R. Yang, Z. Lei, C. Chen, and C. Zheng, "Experimental study on blasting energy distribution and utilization efficiency using water jet test," *Energies*, vol. 1320 pages, 2020.

[22] Y. Guo, Q. Li, R. Yang, P. Xu, Y. Wang, and S. Huo, "Study on crack propagation law of cylindrical charges in three-dimensional models," *Journal of Vibration and Shock*, vol. 39, no. 10, pp. 133–140, 2020.

[23] A. R. Hajibagherpour, H. Mansouri, and M. Bahaaddini, "Numerical modeling of the fractured zones around a hole," *Computers and Geotechnics*, vol. 123, 2020.

[24] R. Yang, C. Ding, Y. Wang, and C. Chen, "Action-effect study of medium under loading of explosion stress wave and explosion gas," *Chinese Journal of Rock Mechanics and Engineering*, vol. 35, pp. 3501–3506, 2016.

[25] Y. Guo, Q. Li, R. Yang, P. Xu, Y. Zhao, and Y. Wang, "Evolution of stress field in cylindrical blasting with bottom initiation," *Optics and Lasers in Engineering*, vol. 133, Article ID 106153, 2020.

[26] X. Lou, P. Zhou, J. Yu, and M. Sun, "Analysis on the impact pressure on blast hole wall with radial air-decked charge based on shock tube theory," *Soil Dynamics and Earthquake Engineering*, vol. 128, 2020.

[27] L. Yang, C. Ding, R. Yang, and Q. Wang, "Experimental and theoretical analysis of stress superposition in double-hole blasts," *Journal of Testing and Evaluation*, vol. 48, no. 5, 2020.

[28] R. Yang, C. Ding, L. Yang, C. Chen, and J. Sun, "Tests for structures with flaws under impact loading," *Journal of Vibration and Shock*, vol. 35, no. 15, pp. 103–108, 2016.

[29] R. Yang, Y. Guo, Q. Li, P. Xu, C. Chen, and S. Fang, "Evolution law on explosive stress and strain field of cylindrical charges at middle detonation position," *Journal of the China Coal Society*, vol. 44, no. 11, pp. 3423–3431, 2019.

[30] L. F. Triviño, B. Mohanty, and B. Milkereit, "Seismic waveforms from explosive sources located in boreholes and initiated in different directions," *Journal of Applied Geophysics*, vol. 87, pp. 81–93, 2012.

[31] T. V. Do, T. M. Pham, and H. Hao, "Stress wave propagation and structural response of precast concrete segmental columns under simulated blast loads," *International Journal of Impact Engineering*, vol. 143, Article ID 103595, 2020.

[32] D. Balkan, Ö Demir, and A. Arıkoğlu, "Dynamic analysis of a stiffened composite plate under blast load: a new model and experimental validation," *International Journal of Impact Engineering*, vol. 143, Article ID 103591, 2020.

[33] A. N. Pratomo, S. P. Santosa, L. Gunawan, D. Widagdo, and I. S. Putra, "Numerical study and experimental validation of blastworthy structure using aluminum foam sandwich subjected to fragmented 8 kg TNT blast loading," *International Journal of Impact Engineering*, vol. 146, Article ID 103699, 2020.

[34] S. H. Chen, M. Y. Wang, Y. T. Zhao, and Q. H. Qian, "Time-stress history on interface between cracked and uncracked zones under rock blasting," *Chinese Journal of Rock Mechanics*, vol. 11, pp. 1784–1788, 2003.

[35] W. I. Duvall and I. Wilbur, "Strain-wave shapes in rock near explosions," *Geophysics*, vol. 18, no. 2, pp. 310–323, 1953.

[36] R. F. Favreau, "Generation of strain waves in rock by an explosion in a spherical cavity," *Journal of Geophysical Research*, vol. 74, no. 17, pp. 4267–4280, 1969.

[37] Y. Zhang, Y. Jiang, D. Asahina, and C. Wang, "Experimental and numerical investigation on shear failure behavior of rock-like samples containing multiple non-persistent joints," *Rock Mechanics and Rock Engineering*, vol. 53, pp. 4717–4744, 2020.